Multimodal Hyperspectral Optical Microscopy

Irina V. Novikova,[1] Chuck R. Smallwood,[1] Yu Gong,[2] Dehong Hu,[1] Leif Hendricks,[3] James E. Evans,[1] Ashish Bhattarai,[2] Wayne P. Hess,[2] Patrick Z. El-Khoury[2]*

[1]Environmental and Molecular Sciences Laboratory, and [2]Physical Sciences Division, Pacific Northwest National Laboratory, P.O. Box 999, Richland, WA 99354, USA;

[3]Surface Optics Corp., 11555 Rancho Bernardo Rd., San Diego, CA 92127, USA.

ABSTRACT

We describe a unique approach to hyperspectral optical microscopy, herein achieved by coupling a hyperspectral imager to various optical microscopes. Hyperspectral fluorescence micrographs of isolated fluorescent beads are first employed to ensure spectral calibration of our detector and to gauge the attainable spatial resolution of our measurements. Different science applications of our instrument are then described. Spatially over-sampled absorption spectroscopy of a single lipid (18:1 Liss Rhod PE) layer reveals that optical densities on the order of 10-3 can be resolved by spatially averaging the recorded optical signatures. This is followed by three applications in the general areas of plasmonics and bioimaging. Notably, we deploy hyperspectral absorption microscopy to identify and image pigments within a simple biological system, namely, a single live Tisochrysis lutea cell. Overall, this work paves the way for multimodal spectral imaging measurements spanning the realms of several scientific disciples.

KEYWORDS: Multimodal Optical Microscopy, Hyperspectral Optical Microscopy, Bioimaging, Spectral Imaging Microscopy

INTRODUCTION

Recent advances in optical spectroscopy, microscopy, and their combinations have greatly advanced our understanding of fundamental processes of relevance to energy, environmental, and biological sciences [1,2]. In the realm of optical micro-spectroscopy, fluorescence is by far the most widespread and well-established imaging contrast mechanism; even few-molecule fluorescence line-scan images were recorded as early as 1976 [3]. It is interesting to compare the latter with single molecule (the ultimate) detection sensitivity obtained in (i) optical absorption-based imaging experiments, initially in a solid held at 1.6 K [4] and subsequently under ambient laboratory conditions [5,6,7], which eluded practitioners over 1 and 2 additional decades, respectively, and (ii) Raman imaging measurements [8], which still comprise a topic of great interest and active research [9,10,11]. Overall, the aforementioned biological and chemical imaging technologies are ever-evolving. For instance, various flavors of fluorescence microscopy, including laser scanning confocal, two-photon, super-resolution, and single molecule-based imaging have been developed over the years and have transformed the way we visualize micro and nanoscopic analytes, particularly in the life sciences [12,13,14,15]. Of relevance to the present study are recent reports of hyperspectral fluorescence imaging capabilities, primarily geared towards biological applications [16,17,18,19,20,21,22]. Fluorescence imaging technologies however suffer from several inherent limitations, the most mundane of which has to do with the fact that most molecules in nature absorb and scatter, but do not fluoresce [23]. The need for novel microscopic and micro-spectroscopic tools that rely on different contrast mechanisms to visualize, e.g., unlabeled biological systems as well as non-fluorescent metal nanoparticles and/or molecular

systems presents itself in this context [5-7,23,24]. The latter is evident in recent and ongoing efforts aimed at advancing novel imaging methodologies based on linear, nonlinear, and/or surface-plasmon-enhanced vibrational and electronic spectroscopy [23,25,26,27,28,29,30].

Besides fluorescence-based super-resolution optical imaging methods [15], far-field optical scattering and absorption techniques are generally diffraction limited. The latter-mentioned experiments are nonetheless relatively straightforward to setup and are potentially greatly informative, particularly if spectroscopic information is encoded in each pixel, i.e., in spectral imaging measurements [31,32,33,34]. In addition to hyperspectral fluorescence imaging [16-22], spectrally resolved dark field optical microscopy [35,36,37,38,39] comes to mind in this context; prior works [35-39] explored the information content in dark field spectral images of individual and interacting plasmonic nanostructures of different shapes and sizes in various media. Our recently reported approach to hyperspectral dark field optical microscopy [39] relied on the combination of a portable hyperspectral imager and a conventional dark field microscope. What distinguishes our approach [39] from previously described analogues is that it requires neither sample scanning, light source spatial/spectral scanning, nor point by point detection schemes, which (i) are typically more time consuming and as a result may introduce uncertainties (e.g. as a result of image drift under ambient laboratory conditions), (ii) often involve more convoluted setups and subsequent numerical analyses, and (iii) involve more costly hardware. The aforementioned advantages are carried over to the present work, in which we build on and significantly expand the scope of our prior report [39]. Namely, we describe diffraction-limited hyperspectral

fluorescence, dark field, as well optical absorption microscopy measurements. Our experimental and data analysis schemes are illustrated through exemplary measurements targeting samples that are strategically selected to explore the advantages and limitations of our approach to multimodal hyperspectral optical microscopy.

EXPERIMENTAL SECTION

Hyperspectral Detector and Data Acquisition. The described hyperspectral optical microscopy (HOM) measurements are based on a hyperspectral imager (Surface Optics, SOC710-VP), which can be coupled to any research grade optical microscope through a standard C-mount. Three dimensional (3D) HOM images are recorded by (i) projecting a narrow line of an optical micrograph onto a 30 μm-wide slit, (ii) dispersing the slit image through a grating onto a 2D (x,y) sensor array (1392×1040 pixels, Sony HAD), and (iii) scanning the slit across the image plane to span the second spatial dimension. Our imager is equipped with an internal slit scanner. As such, 3D image cubes are recorded without the need for sample stage scanning. Binning (factors of 8 and 2 in the 1040 spectral and 1392 spatial dimensions) and subsequent truncation of data points in the spectral and spatial dimensions (1 and 88 from each edge of the detector, respectively) followed by scanning the slit over 696 lines results in a 696x520x128 hyperspectral image cube, which is recorded at a rate of 25-120 s/full cube. The recorded images are spatially calibrated using NIST-traceable standards; using a 100X objective, the resulting diffraction-limited HOM image cubes are sampled at 84 nm^2/pixel over a field of view of 43.7 μm x 58.5 μm.

Light Source Considerations. Much like in standard optical microscopy, any broad band light source (e.g. a tungsten-halogen lamp) may be used to record bright/dark field HOM images. That said, with losses through the optical components (chiefly the objective) along the light path and the overall detector efficiency in mind, the choice of light source becomes an important consideration. To take advantage of the full spectral range of the detector, we employ a broad band incoherent laser-driven light source (EQ-1500 LDLS, Energetiq Technology Inc.), unless otherwise indicated. Our LDLS features high spectral irradiance (up to > 10 $mW/mm^2/nm/sr$) and a quasi-flat profile across a broad spectral range spanning the deep-ultraviolet (measured down to 180 nm) to the near-IR (measured up to 1200 nm). The choice of light source used was made empirically; we tested out various commercial sources including a variety of tungsten-halogen lamps, mercury vapor lamps, and light emitting diodes. The flat spectral profile and high irradiance of our LDLS proved superior for the purposes of our bright and dark field HOM measurements.

Data Analysis. While fluorescence micrographs recorded using suitable laser sources (herein continuous wave lasers at 473, 532, and 630 nm) and filters (500-550 band pass, 570 long pass, and 690 long pass, respectively) are essentially background free, transforming spectrally-resolved intensity images into hyperspectral absorption or dark field image cubes requires a few additional steps. For instance, obtaining a hyperspectral absorption micrograph from a transmitted light bright field spectral image would require measuring a reference '$I_0(x,y,\lambda)$' cube, whereby e.g., light is transmitted through a thin coverslip that supports the target. Much like in standard absorption spectrometry, we then take $-\log_{10}(I_{sample}(x,y,\lambda)/I_0(x,y,\lambda))$, in which $I_{sample}(x,y,\lambda)$ corresponds to the spatially

(down to 84 nm^2/pixel at 100X) and spectrally (377-1051 nm, $\Delta\lambda \approx 5$ nm) resolved intensity across the sample image plane, and $I_0(x,y,\lambda)$ denotes the hyperspectral image of the background. Reflectance and dark field spectral micrographs can be similarly obtained as $I_{sample}(x,y,\lambda)/I_0(x,y,\lambda)$, where $I_0(x,y,\lambda)$ are reference spectral image cubes recorded using specular and diffusive reflection standards, respectively. Overall, our analysis schemes ensure that the spectral micrographs of the sample are not affected by (i) the spatial/spectral characteristic of the light source, (ii) intensity losses along the optical path, and (iii) the overall efficiency of our detector. The resulting image cubes are essentially internally calibrated.

Helium Ion Microscopy. Our helium ion microscope (Zeiss Orion) was operated at an optimal imaging voltage of 30 kV, an aperture size of 10 μm, a spot size of 4 μm, and a beam blanker current of 0.5-1.5 pA. An Everhart-Thornley (E-T) detector was used to image the samples. The working distance was varied in the 5-8 mm range.

Sample Preparation. *The first sample* consists of tetraspeck beads of 200 nm in diameter (ThermoFisher Scientific), drop casted onto a 0.1 mm-thick glass coverslip. These spherical beads are infused with four different fluorescent dyes, yielding nanoscopic targets that display 4 different manufacturer-specified excitation/emission peaks at 360/430 nm, 505/515 nm, 560/580 nm, and 660/680 nm. *The second and third samples* are similarly prepared by drop casting citrate stabilized silver nanoparticles of ~100 nm in diameter (Sigma-Aldrich) onto either (i) a 0.1 mm-thick glass coverslip, or (ii) a corrugated 20 nm-thick silver film (~5 nm surface roughness) sputtered onto a glass coverslip by arc-discharge physical vapor deposition (Cressington 208HR, target: Ted Pella Inc., 99.99% purity). *The fourth sample* was similarly prepared by coating a

commercial silicon atomic force microscopy probe (Nanosensors, ATEC; 20 nm radius of curvature) with 35 nm of silver. The tip was subsequently immobilized on a glass substrate with the cantilever pointing away from the support. *The fifth sample* comprises a single layer of 18:1 Liss Rhod PE (Avantilipids), deposited using a Langmuir-Blodgett trough (model 611B) on a 0.1 mm-thick glass coverslip. The glass substrate was first immersed in water, followed by spreading 30 μL of a 1 mg/mL $CHCl_3$ solution of the lipid at the water air interface. The lipid layer was subsequently compressed to a surface pressure of 18 mN/m and maintained at that pressure throughout the monolayer coating process, which was achieved by pulling the slides at a rate of 3 mm/minute. For *the sixth sample, Tisochrysis lutea* cells were grown under phototropic conditions in Keller medium cultured with a 12 hour diurnal cycle using 12 hour light entrainment with 470 nm and 650 nm LED light sources (~9 mW total power, ~80 μmoles of photons m^{-2} s^{-1}) [40]. Cells were harvested at late log growth and concentrated by centrifuging an aliquot at 700G for 2 mins prior to drop casting 3μL of the culture onto a poly-lysine coated microscope slide. The sample was subsequently enclosed using a 0.17 mm glass coverslip prior to conducting the optical measurements.

RESULTS AND DISCUSSION

Hyperspectral Fluorescence (HF) Microscopy. HF micrographs of a sparse distribution of tetraspeck beads cubes were recorded using a wide field fluorescence microscope (Zeiss AxioObserver) equipped with a 100X oil immersion objective (numerical aperture = 1.4). The recorded 3D micrographs contain both spatial and spectral information and can be analyzed by taking image slices at different wavelengths and/or by inspecting the

spectra at each pixel [39]. Selected image slices extracted from 3 different HF image cubes recorded following 473, 532, and 660 nm laser irradiation are shown in Figure 1. The three images track the same set of particles near the emission maxima of the different fluorophores with which they are infused. The enumerated particles are further analyzed in Figures 2 and 3. Figure 2 shows the spectral response in a selected region of the HF image cube that contains a single fluorescent bead (particle 7 in Figure 1). Shown in Figure 2A-C are individual pixel (84 nm^2/pixel) as well as spatially averaged (3×3 pixel area) spectra of the same particle. Ample signal to noise is obtained in the spatially averaged fluorescence spectra; the recorded signal maxima are consistent with the manufacturer-provided values of 515, 180 and 680 nm, within the spectral resolution of our detector (< 5 nm). A horizontal fluorescence cross-section at excitation/emission wavelengths of 532/580 nm is shown in Figure 2D. A Gaussian fit to the recorded intensity profile indicates a full width at half maximum of 280 ± 8 nm, which (i) is consistent with the theoretical value of $(0.61 \times 580) / 1.4 \approx 253\ nm$, and (ii) ensures that the spectra are that of a single bead. The above-described analysis was then performed to extract diffraction-limited spectra of the particles highlighted in Figure 1 (particles 1-17). The results are shown in Figure S1 of the supporting information section, which also illustrates the average fluorescence signal of all 17 particles considered in this analysis. Overall, our HF measurements illustrate that (i) HF microscopy is feasible by coupling our hyperspectral detector to a wide field fluorescence microscope, (ii) our detector is spectrally calibrated, (iii) diffraction limited images may be extracted from the recorded HF image cubes, and (iv) single fluorescent beads can be analyzed one particle at a time *via* HF microscopy. Evidently, a camera optimized for fluorescence spectroscopy would

be needed to detect nominally weaker fluorophores; the latter is nonetheless not the goal of this report. Rather, in the following, we illustrate that (iii) and (iv) may also be achieved by relying on the ground to excited electronic state transitions of the embedded fluorophores.

Hyperspectral Optical Absorption (HA) Microscopy. Shown in Figure 3A is a selected region of the HA image cube that contains the same fluorescent bead analyzed in Figure 2. These measurements were performed using 100X microscope objective with a numerical aperture of 0.8. We again extract a total of 9 single pixel spectra (3×3) and their average, as illustrated in Figure 3B. Inspection of the absorption spectra of the single bead reveals that the absorption signals of the red chromophores with excitation maxima at 660 and 560 nm are convolved; only a single broad absorption peak is observable in the 525-750 nm spectral region. The blue chromophore however exhibits a single absorption maximum a ~488 nm. A horizontal absorption profile taken towards the center of the fluorescent bead at the absorption maximum is shown in Figure 3C. A Gaussian fit to the recorded intensity profile indicates a full width at half maximum of 370 ± 10 nm, which again (i) is consistent with the theoretical value of $(0.61 \times 488) / 0.8 \approx 372\ nm$, and (ii) ensures that the recorded spectra are that of a single bead. We repeat the above-described single particle analysis to extract the spatially averaged single particle spectra (1-17 in Figure 1), which are shown in Figure 3D along with the average absorption from all particles. These results are consistent with the HF measurements and observables therein; slight variations in the optical properties of the various particles are evident, but the overall spectra are similar. These measurements further suggest that fluorescent molecular ensembles can be identified and imaged by relying on their optical

(electronic) absorption in a HA microscopy scheme. In an ensuing section of this work, we will take advantage of the latter-mentioned feature to identify and image native fluorophores within a single live cell.

Hyperspectral Dark Field (HDF) Optical Microscopy. Our recent report of HDF optical microscopy [39] targeted prototypical silver nanospheres (100 nm diameter) dispersed on a glass microscope slide. The attainable signal-to-noise in the recorded spectral images allowed us to examine and image one plasmonic silver nanoparticle at a time [39]. Analysis of the scattering spectra of 31 different nanoparticles revealed marked differences between the optical properties of the nanospheres, including their (i) relative scattering efficiencies, (ii) surface plasmon resonance maxima, and (iii) derived peak widths. While (iii) is directly related to the dephasing of the coherent electron oscillations [41], (i) and (ii) are associated with nanometric imperfections in the structures of the plasmonic particles [39,42,43]. The latter is exemplified in the measurements shown in Figure S2 of the supporting information section and Figure 4, whereby 100 nm plasmonic silver nanoparticles deposited either on a glass or a corrugated (~5 nm rms surface roughness) silver thin film are interrogated by HDF microscopy. The results shown in Figure 2S are similar to those of our previous report [39], to which the reader is referred for a more detailed analysis. Figure 4 however shows that although the averaged plasmonic response (thick solid red line) of the nanoparticles on the metal thin film strongly resembles its analogue that was recorded on the glass substrate (thick solid red line in Figure 2S), the individual particle spectra comprising the former construct exhibit dramatic spectral variations. These include well-defined resonances in the 500-675 nm spectral region, a few of which are highlighted using red arrows in Figure 4B, and

attributed to hybrid nanoparticle-corrugated metal film plasmonic resonances. These localized surface plasmon resonances are governed by the varying local topology of the corrugated metal film with which each particle is interacting. Interestingly, the averaged optical response masks the heterogeneity of the scattering spectra of the individual particles, which in effect broadcast interactions taking place over length scales much finer than the spatial resolution attainable using the all-optical technique described herein [39,42,43]. In a similar experiment, we correlate helium ion images of an Ag-coated atomic force microscopy tip with HDF micrographs of the same tip, see Figure 5. Similar tips are often used in tip-enhanced Raman spectroscopy (TERS)-based nanoscale chemical imaging and analysis [34]. Herein, we illustrate that HDF optical microscopy can be used as a routine tool to measure the characteristic plasmon resonances of such metallic probes. A hyperspectral image slice at the plasmon resonance maximum (417 nm) of the tip (Figures 5B) and subsequent spectral slices (Figures 5C and 5D) allow us both to locate the apex of the tip in 3D space and to measure its characteristic resonance. This all-experimental analysis is particularly valuable for TERS practitioners, as most of the existing knowledge of the plasmonic response of the probes is based on numerical simulations that assume idealized tip shapes. In practice nanometric corrugations that are sustained on TERS probes (evident in Figure 5A) are expected to affect the properties of the tip, and hence, the recorded enhanced Raman spectra and images. Our approach in invaluable in this regard.

Spatially-Oversampled Absorption Spectroscopy of Continuous Samples. Besides single particle combined spatial-spectral analysis, our approach can also be used to record ultrasensitive optical spectra of continuous samples. This may be readily achieved by

averaging the optical spectra recorded at different spatial positions, essentially yielding a spatially oversampled optical response of a sample of interest. To illustrate the principle, we recorded the transmitted light optical absorption hyperspectral image of a lipid (18:1 Liss Rhod PE) monolayer on a glass coverslip. Spatial averaging over 3120 single pixel spectra (520 pixels/lines×6 lines) yields the absorption spectrum shown in Figure 6. Several observations are noteworthy. First and foremost, spatial averaging increases the signal to noise ratio and allows us, in this example, to reliably resolve optical densities on the order of $\sim 1\times10^{-3}$ in the 450-650 nm spectral region. Notably, we only average < 10% of the pixels which comprise the recorded spectral image to obtain the demonstrated level of sensitivity; the smallest measureable signal using this approach is yet to be determined. Second, the monolayer absorption spectrum exhibits several differences when compared to a standard visible absorption spectrum recorded from a dilute lipid/$CHCl_3$ solution. For instance, a 21 nm red-shifted absorption maximum is observed when the lipid spectrum is compared to its solution-phase analogue (580 *vs* 559 nm). As the dielectric constants of the solvent (4.81) and the coverslip (~5) are comparable, the observed red-shift is indicative of strong intermolecular interactions in the lipid monolayer. In the same vein, the lowest energy excited vibronic bands observable in both the lipid (544 nm) and solution (525 nm) spectra are suggestive of modified topologies in the Franck-Condon regions of the excited electronic states in the two cases. Namely, the derived excited vibronic state frequencies are 1159 and 1141 cm^{-1} in the solvated species and molecular film, respectively; the potentials of the optically accessible excited vibronic states are stiffened in the latter. Further insights into the exact intermolecular interactions that lead

to the aforementioned differences in the two cases would require further experimental and theoretical investigations that stem beyond the scope of this work.

Single Cell Imaging *via* HA Microscopy. That fluorescent molecular ensembles can be addressed through their ground to excited electronic state transitions in a HA microscopy scheme is advantageous from a biological imaging perspective [24]. To illustrate the concept, we recorded HA micrographs of a single live *Tisochrysis lutea* cell, see Figures 7 and 8. Recent efforts aimed at exploring high lipid accumulating strains of oleaginous algae identify *Tisochrysis lutea* as a candidate for maximizing neutral lipid content for biofuel feedstocks [44,45,46]. To explore some of the information content of the recorded HA micrographs of *Tisochrysis lutea*, we rely on three key pioneering works [47,48,49]. The first report explored algal pigments, and reported the *in vivo* specific absorption coefficients of chlorophylls and carotenoids [47]. The authors found that whereas chlorophylls A, B, and C as well as carotenoids all absorb in the 400-500 nm spectral region, only carotenoids are responsible for optical absorption in the 500-550 nm range [47]. The second report [48] reveals that under the growth conditions used in our present work, the optical signatures of chlorophyll A and carotenoids are expected to dominate the spectral images. Namely, the chlorophyll C content in *Tisochrysis lutea* cells is expected to be minimal under phototropic growth conditions [48]. In the third work, transmission electron micrographs of closely related systems, including *Tisochrysis lutea* sp. nov., were recorded [49]. Of the various subcellular compartments that were identified and visualized [49], the plastid was found to be crescent-shaped and traces the outer cell membrane of a nearly spherical cell of 4-6 μm in diameter.

Figure 7A shows the 518 nm absorption image of a live *Tisochrysis lutea* cell immobilized on a poly-lysine coated microscope slide. As carotenoids are the primary absorbing pigments at this wavelength [47], regions of high absorption (red) correspond to regions of the cell to which carotenoids are localized. Not surprisingly, the carotenoid absorption map essentially traces the plastid [49]. A comparison of two single pixel spectra taken at (i) the plastid, and (ii) towards the center of the cell further illustrate the distinct optical signatures in different regions of the cell, see Figure 7B. Namely, whereas the spectrum recorded at (i) is dominated by the optical response of carotenoids [47], spectrum at (ii) is essentially a convolved response from the various algal pigments. The latter effect is even more evident in the global analysis of the HA micrograph of the imaged cell, see Figure 8. The 503 nm absorption image of the same cell is shown Figure 8A, and absorption profiles tracing the indicated horizontal and vertical profiles (dashed lines) at the same wavelength are shown in Figure 8B. Besides the plastid, other subcellular components, the rigorous unambiguous assignments of which would require further works, are observable in the 503 nm image, see Figure 8A. The full spectral response at each of the individual pixels tracing the horizontal and vertical profiles highlighted in Figure 8A can be visualized in the 2D contour profiles shown in Figures 8C and 8E. We also compare selected single pixel spectra at the positions marked by dashed horizontal lines in Figures 8C and 8E in Figures 8D and 8F, respectively. These spectra reveal that although the blue region of the spectrum is broad and congested, as several pigments absorb in the 400-500 nm range [47], the well-defined chlorophyll A red absorption maximum at ~675 nm can be used to image the spatial distribution of this pigment intracellularly. The 675 nm absorption image (not shown) is similar to the image

shown in Figure 7A, and reveals that much like the carotenoids, chlorophyll A molecules are chiefly localized at the plastid. Overall, our above-described preliminary single cell HA wide-field imaging measurements are encouraging. Namely, our observables are similar to previously described HF single cell point scanning confocal imaging measurements of other algal cells [21], but insights herein are gained using optical absorption contrast in spectral imaging experiments. As such, the above results pave the way for identifying and imaging non-fluorescent macromolecules and small molecules including, e.g., hemoglobin and cytochromes which efficiently absorb visible light but do not efficiently fluoresce as a result of ultrafast non-radiative decay pathways in such (and structurally related) systems. It is important to concede that a single cell in a controlled medium is very different from a real life biological sample where scattering media typically obfuscate the recorded extinction-based spectral images. That said, using a single optical microscope that is capable of both scattering and absorption measurements would allow us to distinguish between the total extinction (in absorption mode) from the pure scattering (in dark field mode) response. The aforementioned demonstrations suggest that the current incarnation of the hyperspectral imager used in this study can be adopted to accomplish the latter.

CONCLUSIONS AND OUTLOOK

This work describes spectrally and spatially resolved fluorescence, dark field, and optical absorption microscopy measurements targeting several model systems, including (i) single fluorescent nanospheres, (ii) single plasmonic nanoparticles residing in varying local environments, (iii) a plasmonic atomic force microscopy tip, (iv) a lipid (18:1 Liss Rhod PE) monolayer, and (v) an isolated live *Tisochrysis lutea* cell. Although elegant

demonstrations of hyperspectral fluorescence [16-22] and dark field [35-39] microscopy have been previously reported, hyperspectral optical absorption microscopy experiments are scarce, particularly in the realm of biological imaging. We concede the limitations of the approach described in this work. First, the limited signal-to-noise ratio of the CCD camera used in our measurements limits the range of target systems that can be addressed using the various imaging contrasts demonstrated herein. In this regard, our team is currently working on interfacing the hyperspectral imager with a more sensitive/spectroscopic grade CCD camera. This is particularly needed for fluorescence and nonlinear optical micro-spectroscopy measurements. Second, achieving multimodal (fluorescence, absorption, dark field, nonlinear) hyperspectral optical microscopy from the sample would require a microscope that simultaneously supports all of the aforementioned imaging modalities. A home built optical microscope that achieves the latter is currently under construction in our laboratory.

AUTHOR INFORMATION

[*]patrick.elkhoury@pnnl.gov
Pacific Northwest National Laboratory
902 Batelle Boulevard
P. O. Box 999, MSIN K8-88
Richland, WA 99354, USA
Tel: 509-371-6048
Fax: 509-371-6145

COMPETING FINANCIAL INTERESTS

The authors declare no competing financial interests.

ACKNOWLEDGMENTS

PZE acknowledges support from the Laboratory Directed Research and Development Program at Pacific Northwest National Laboratory (PNNL). A.B. was supported by the

Department of Energy's (DOE) Office of Biological and Environmental Research (BER) Bioimaging Technology project #69212. YG and WPH are supported by the US Department of Energy (DOE), Office of Science, Office of Basic Energy Sciences, Division of Chemical Sciences, Geosciences & Biosciences. IVN, CRS and JEE were supported by DOE-BER Mesoscale to Molecules Bioimaging Project #66382. This work was performed in EMSL, a national scientific user facility sponsored by DOE's Office of Biological and Environmental Research and located at PNNL. PNNL is operated by Battelle Memorial Institute for the United States Department of Energy under DOE contract number DE-AC05-76RL1830.

FIGURES

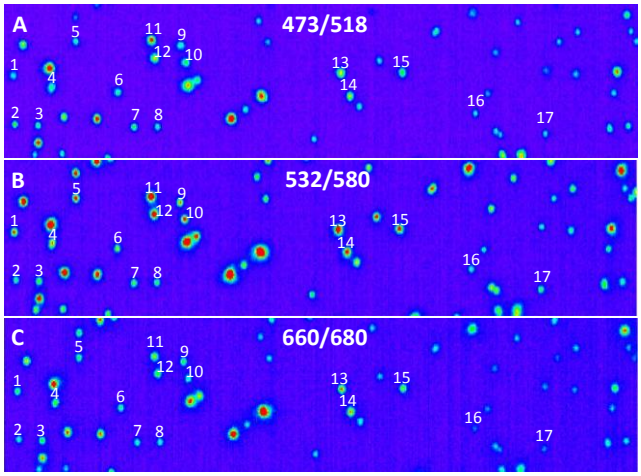

Figure 1. Wide field fluorescence images of a sparse distribution of 200 nm tetraspeck beads on glass at 518 (panel A), 580 (panel B), and 680 (panel C) nm, recorded following 473 (panel A), 532 (panel B), and 660 (panel C) nm continuous wave laser excitation (~1 mW/μm^2), respectively. Note that the images shown in all three panels were taken from a stack of 128 images forming a hyperspectral image cube; the wavelengths chosen for visualization correspond to the fluorescence maxima of three different chromophores selectively excited using our three different laser excitation wavelengths. The field of view in all three panels is 44×10.5 μm^2. The rainbow color scheme used throughout this figure is set such that blue and red correspond to 0 and 200 counts per 500 ms, respectively. The enumerated particles are further analyzed in subsequent figures.

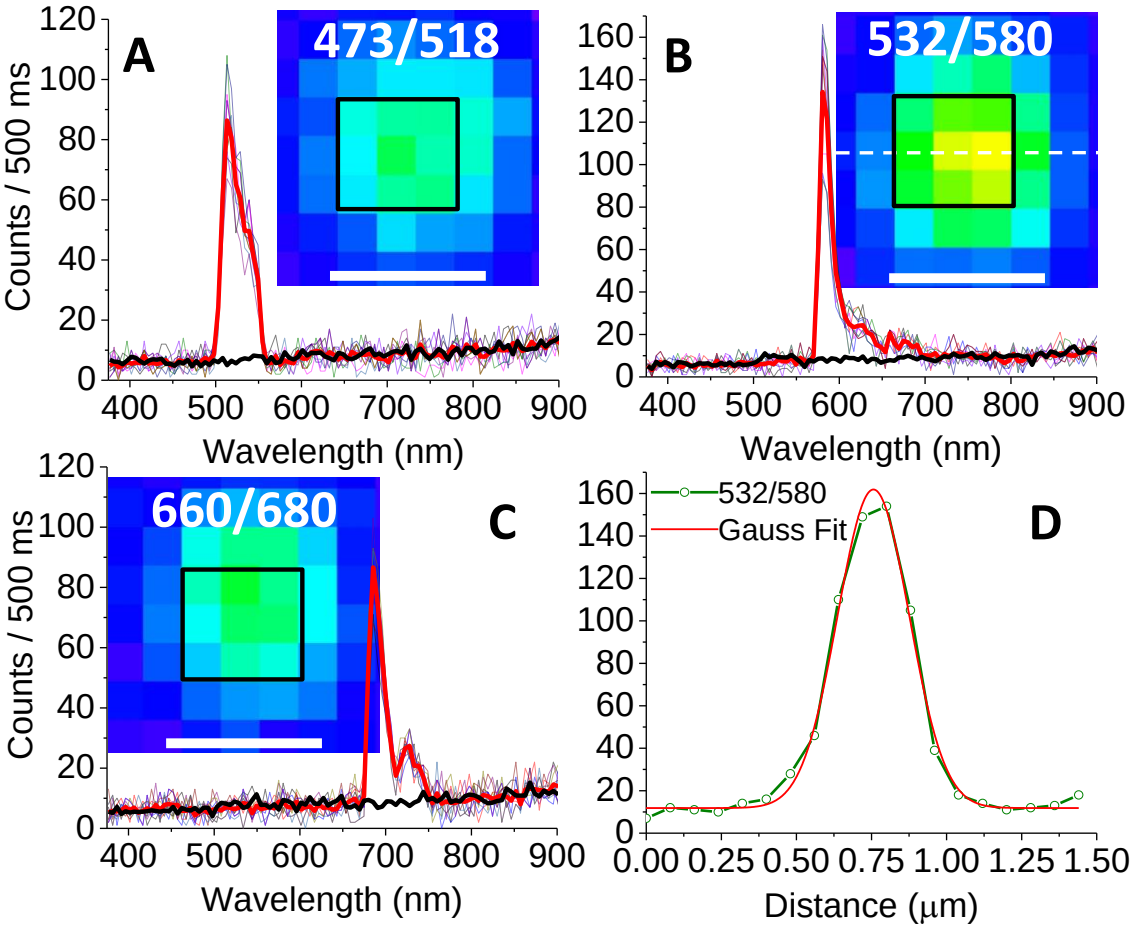

Figure 2. Panel A-C illustrate spatially averaged (3×3 pixel area, thick red line) and individual pixel (thin lines) fluorescence spectra in the regions of interest highlighted using black squares in the inset. Background (thick black line) spectra recorded at a nearby region of the flat glass substrate are shown on the same plots. The images shown in the insets track a single particle (7 in Figure 1) at the designated excitation/emission wavelengths (nm), and the scale bar therein indicates 336 nm. Panel D shows a fluorescence intensity profile taken from the center of the isolated tetraspeck bead (dashed line in panel B). A Gaussian fit (full width at half maximum = 280 ± 8 nm) of the experimental trace is shown in the same panel.

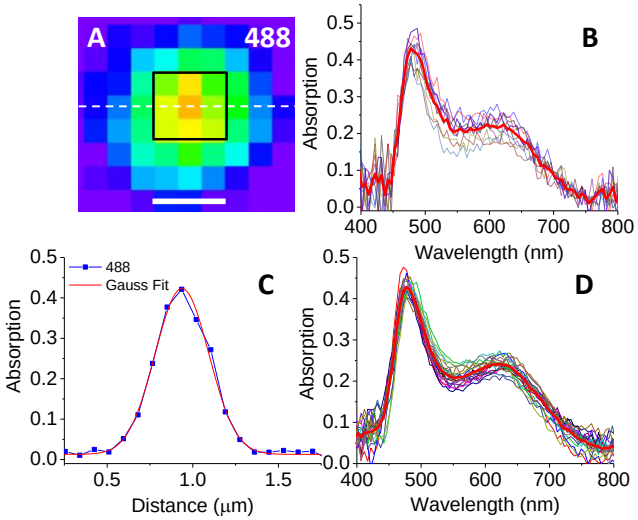

Figure 3. Panel A shows a 488 nm absorption image of the same particle analyzed in Figure 2. The black square highlights a region of interest from which single pixel (thin lines in panel B) and spatially averaged (3×3 pixel area, thick red line in panel C) absorption spectra are taken. A horizontal 488 nm absorption profile is taken towards the center of the image shown, and plotted in panel C, along with its best Gaussian fit (full width at half maximum = 370 ± 14 nm). Spatially averaged (3×3 pixel area) absorption spectra of the 17 tetraspeck beads highlighted in Figure 1 (thin lines) along with the average absorption spectrum of all 17 particles (thick red line) are shown in panel D. The scale bar in the inset of panel A indicates 252 nm.

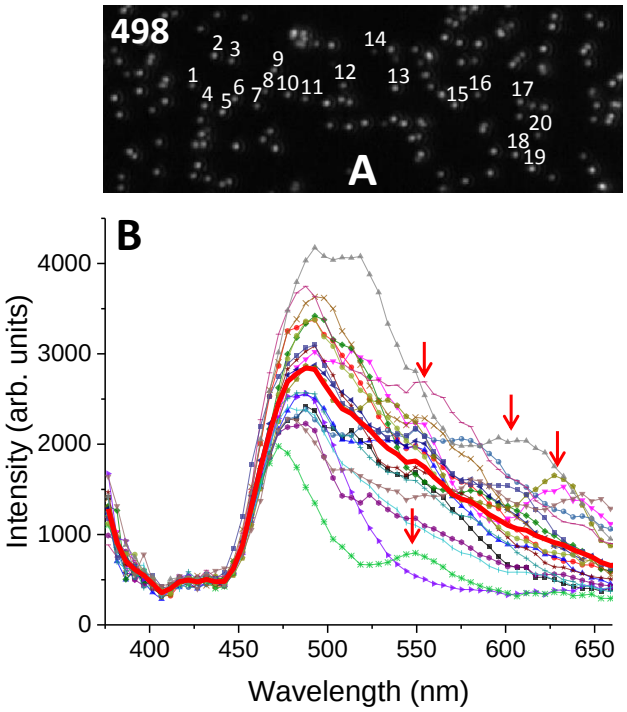

Figure 4. Panel A shows the 498 nm dark field optical image of a sparse distribution of silver nanoparticles of ~100 nm in diameter on a sputtered thin silver film (rms height distribution of ~5 nm). The field of view in this image is 14×31 μm^2. The dark field scattering spectra of the 20 particles highlighted in panel A are spatially averaged (3x3 pixel area) and shown on the same plot in panel B (thin lines and symbols). Also shown in panel B is the average scattering (thick red line) from all 20 particles considered in this analysis.

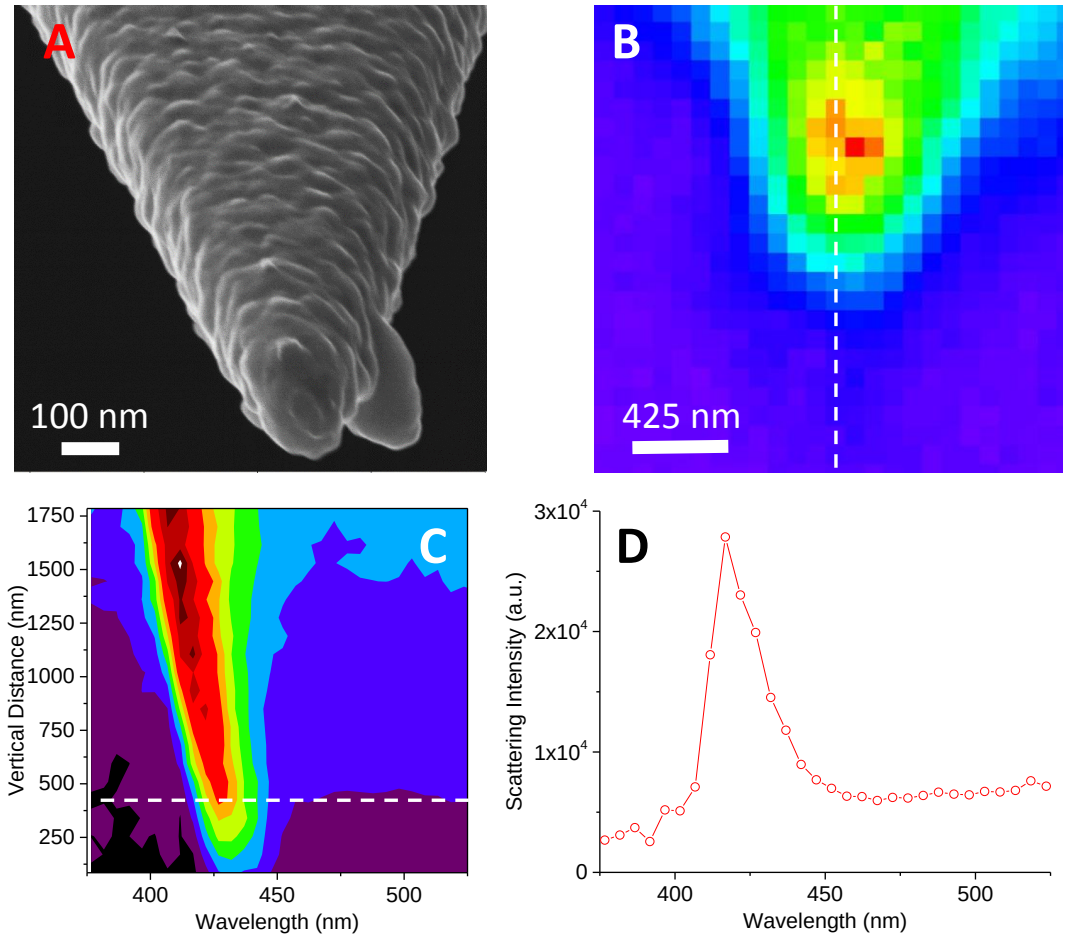

Figure 5. Panel A shows a helium ion image of an AFM tip sputtered with Ag. A hyperspectral dark field image slice (417 nm image) of the same tip is shown in panel B. The dashed vertical line in panel B traces the spatial positions at which the spectral changes are monitored in the 2D contour plot shown panel C. Similarly, the horizontal dashed line in panel C traces the spectral response at the apex of the tip, and it is shown in panel D.

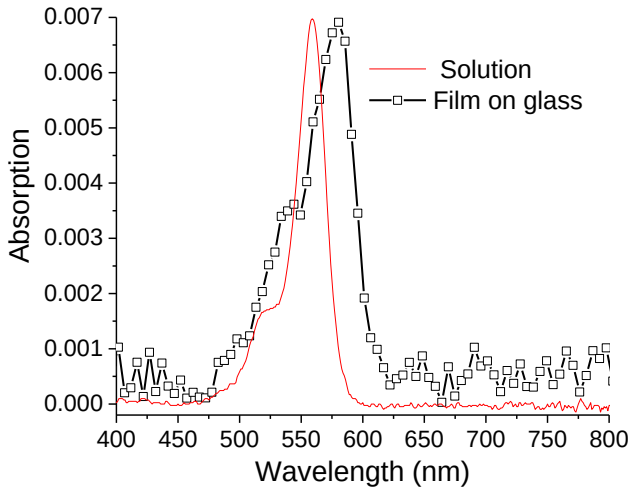

Figure 6. The visible absorption spectrum of an 18:1 Liss Rhod PE monolayer is compared to the bulk absorption spectrum of the same species in $CHCl_3$. Note that the solution spectrum was normalized (1/41X) to fit to scale.

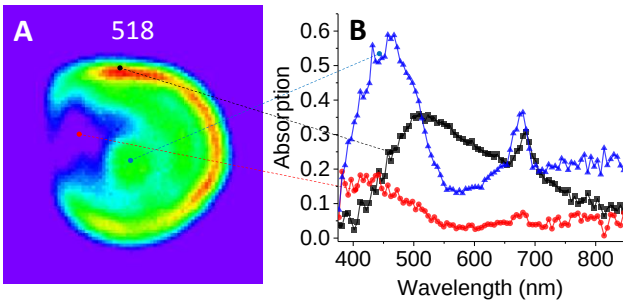

Figure 7. A 518nm absorption image of a live *Tisochrysis lutea* cell residing between a poly-lysine coated microscope slide and a 0.17 mm glass cover slip is shown in panel A. The field of view in this panel is 6.4×6.9 μm^2. Single pixel absorption spectra taken at the positions highlighted in panel A are compared on the same plot in panel B.

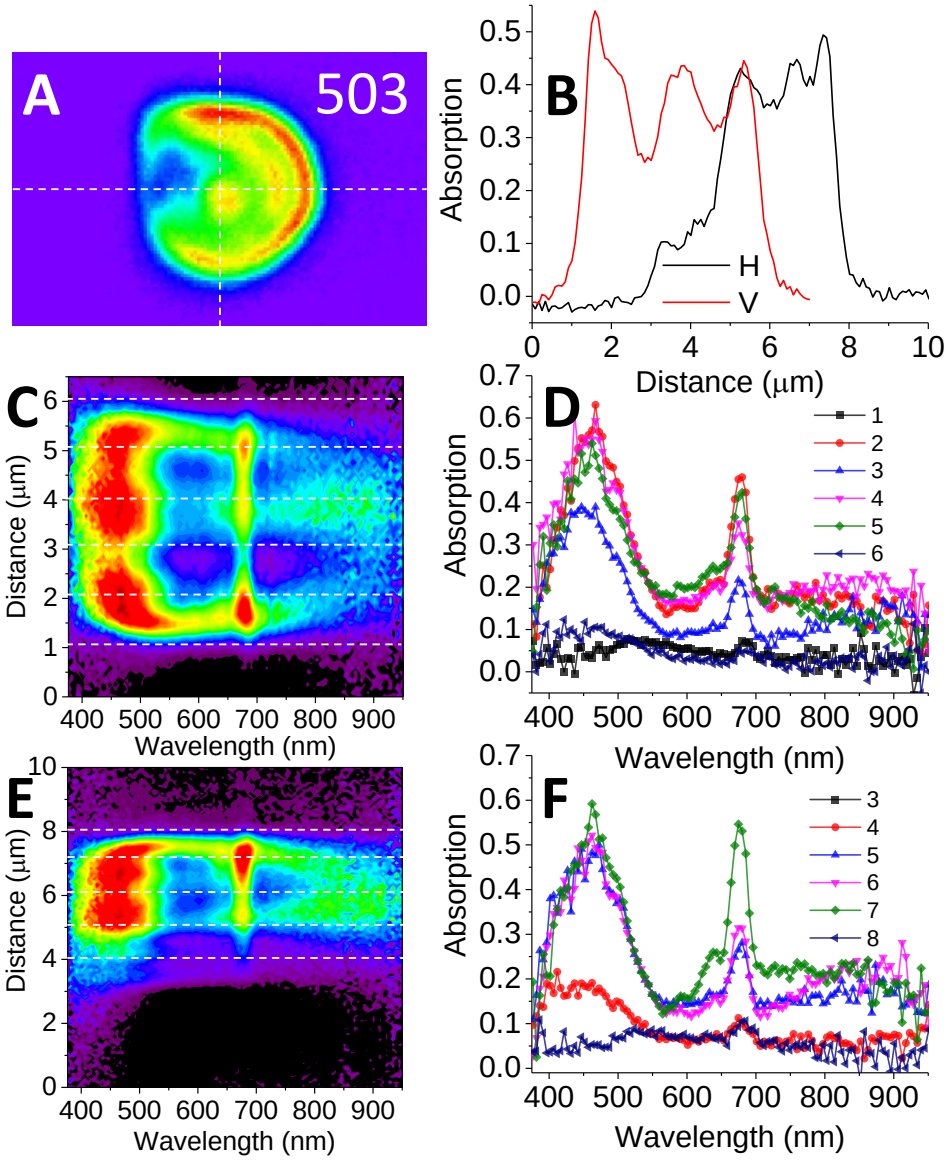

Figure 8. Panel A shows an absorption image of a single *Tisochrysis lutea* cell between a poly-lysine coated microscope slide and a 0.17 mm glass cover slip. The field of view in this panel is 10×7 μm^2, and be readily gauged by inspecting panel B, where horizontal and vertical absorption profiles (dashed lines in panel A) at 503 nm are plotted. Panels C and E show the spatial variation in absorption along the vertical and horizontal directions (dashed lines in panel A), respectively. Select single pixel spectra taken from panels C

and E (spectral cuts highlighted using white dashed lines) are shown in panels D and F, respectively.

TOC Graphic

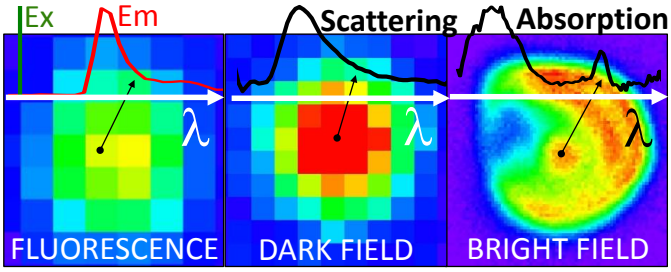
Ex
Em
Scattering
Absorption
λ
λ
λ
FLUORESCENCE
DARK FIELD
BRIGHT FIELD

REFERENCES

[1] Petek, H. Single-Molecule Femtochemistry: Molecular Imaging at the Space-Time Limit. *ACS Nano* **2014**, *1*, 5-13.

[2] Petek, H. Nano meets Femto. *Nature Nanotech.* **2016**, *11*, 404-405.

[3] Hirschfeld, T. Optical Microscopic Observation of Single Small Molecules. *Appl. Opt.* **1976**, *15*, 2965–2966.

[4] Moerner, W. E.; Kador, L. Optical-Detection and Spectroscopy of Single Molecules in a Solid. *Phys. Rev. Lett.* **1989**, *62*, 2535–2538.

[5] Kukura, P.; Celebrano, M.; Renn, A.; Sandoghdar, V. Single-Molecule Sensitivity in Optical Absorption at Room Temperature. *J. Phys. Chem. Lett.* **2010**, *1*, 3323–3327.

[6] Gaiduk, A.; Yorulmaz, M.; Ruijgrok, P. V.; Orrit, M. Room-Temperature Detection of a Single Molecule's Absorption by Photothermal Contrast. *Science* **2010**, *330*, 353–356.

[7] Chong, S.; Min, W.; Xie, X. S. Ground-State Depletion Microscopy: Detection Sensitivity of Single-Molecule Optical Absorption at Room Temperature. *J. Phys. Chem. Lett.* **2010**, *1*, 3316–3322.

[8] Pettinger, B.; Schambach, P.; Villagomez, C. J.; Scott N. Tip-Enhanced Raman Spectroscopy: Near-Fields Acting on a Few Molecules. *Annu. Rev. Phys. Chem.* **2012**, *63*, 379-399.

[9] Pozzi, E.; Sonntag, M.; Jiang, N.; Klingsporn, J.; Hersam, M.; Van Duyne, R. P. Tip-Enhanced Raman Imaging: An Emergent Tool for Probing Biology at the Nanoscale. *ACS Nano* **2013**, *7*, 885–888.

[10] Zhang, R.; Zhang, Y.; Dong, Z. C.; Jiang, S.; Zhang, C.; Chen, L. G.; Zhang, L.; Liao, Y.; Aizpurua, J.; Luo, Y.; et al. Chemical Mapping of a Single Molecule by Plasmon-Enhanced Raman Scattering. *Nature* **2013**, *498*, 82-86.

[11] Park, K. -D.; Muller, E. A.; Kravtsov, V.; Sass, P. M.; Dreyer, J.; Atkin, J. M.; Raschke, M. B. Variable-Temperature Tip-Enhanced Raman Spectroscopy of Single-Molecule Fluctuations and Dynamics. *Nano Lett.* **2016**, *16*, 479-487.

[12] Huang, B.; Bates, M.; Zhuang, X. Super-Resolution Fluorescence Microscopy. *Annu. Rev. Biochem.* **2009**, 78, 993-1016.

[13] Patterson, G.; Davidson, M.; Manley, S.; Lippincott-Schwartz, J. Superresolution Imaging using Single-Molecule Localization. *Annu. Rev. Phys. Chem.* **2010**, *61*, 345-367.

[14] Gahlmann, A.; Moerner, W. E. Exploring Bacterial Cell Biology with Single-Molecule Tracking and Super-Resolution Imaging. *Nat. Rev. Micro.* **2014,** *12*, 9-22.

[15] Hell, S. W. Nobel Lecture: Nanoscopy with Freely Propagating Light. *Rev. Mod. Phys.* **2015**, *87*, 1169-1181.

[16] Davis, R. W.; Jones, H. D. T.; Collins, A. M.; Ricken, J. B.; Sinclair, M. B.; Timlin, J. A.; Singh, S. Label-Free Measurement of Algal Triacylglyceride Production using Fluorescence Hyperspectral Imaging. *Algal Res.* **2014**, *5*, 181-189.

[17] Wang, P.; Ebeling, C. G.; Gerton, J.; Menon, R. Hyper-Spectral Imaging in Scanning-Confocal-Fluorescence Microscopy using a Novel Broadband Diffractive Optic. *Opt. Commun.* **2014**, *324*, 73-80.

[18] Di Caprio, G.; Schaak, D.; Schonbrun, E. Hyperspectral Fluorescence Microfluidic (HFM) Microscopy. *Biomed. Opt. Express* **2013**, *4*, 1486-1493.

[19] Elliott A, D.; Gao, L,; Ustione, A.; Bedard, N.; Kester, R.; Piston, D. W.; Tkaczyk, T. S. Real-Time Hyperspectral Fluorescence Imaging of Pancreatic Beta-Cell Dynamics with the Image Mapping Spectrometer. *J. Cell. Sci.* **2012**, *125*, 4833-4840.

[20] Studer, V.; Bobin, J.; Chahid, M.; Mousavi, H. S.; Candes, E.; Dahan, M. Compressive Fluorescence Microscopy for Biological and Hyperspectral Imaging. *Proc. Natl. Acad. Sci.* **2012**, *109*, 1679-1687.

[21] Vermaas, W. F. J.; Timlin, J. A.; Jones, H. D. T.; Sinclair, M. B.; Nieman, L. T.; Hamad, S. W.; Melgaard, D. K.; Haaland, D. M. In vivo Hyperspectral Vonfocal Fluorescence Imaging to Determine Pigment Localization and Distribution in Cyanobacterial Cells. *Proc. Natl. Acad. Sci.* **2008**, *105*, 4050-4055.

[22] Cutler, P. J.; Malik, M. D.; Liu, S.; Byars, J. M.; Lidke, D. S.; Lidke, K. A. Multi-Color Quantum Dot Tracking Using a High-Speed Hyperspectral Line-Scanning Microscope. *PLoS One* **2013**, *8*, e64320-1-14.

[23] Ortega Arroyo, J.; Kukura, P. Non-Fluorescent Schemes for Single-Molecule Detection, Imaging and Spectroscopy. *Nat. Photonics* **2016**, *10*, 11-17.

[24] Biteen, J. S.; Blainey, P. C.; Cardon, Z. G.; Chun, M.; Church, G. M.; Dorrestein, P. C.; *et al.* Tools for the Microbiome: Nano and Beyond. *ACS Nano* **2016**, *10*, 6-37.

[25] Piatkowski, L.; Gellings, E.; Van Hulst, N. F. Broadband Single-Molecule Excitation Spectroscopy. *Nat. Commun.* **2016**, *7*, 10411. doi:10.1038/ncomms10411

[26] Cheng, J. -X.; Xie, X. S. Vibrational Spectroscopic Imaging of Living Systems: An Emerging Platform for Biology and Medicine. *Science* **2015**, *350*, aaa870-1-9.

[27] Kravtsov, V.; Ulbricht, R.; Atkin, J. M.; Raschke, M. B. Plasmonic Nanofocused Four-wave Mixing for Femtosecond Near-Field Imaging. *Nat. Nanotechnol.* **2016**, *11*, 459-464.

[28] Atkin, J. M.; Sass, P. M.; Teichen, P. E.; Eaves, J. D.; Raschke, M. B. Nanoscale Probing of Dynamics in Local Molecular Environments. *J. Phys. Chem. Lett.* **2015**, *6*, 4616-4621.

[29]Yampolsky, S.; Fishman, D. A.; Dey, S.; Hulkko, E.; Banik, M.; Potma E. O.; Apkarian, V. A. Seeing a Single Molecule Vibrate through Time-Resolved Coherent Anti-Stokes Raman Scattering. *Nat. Photonics* **2014**, *8*, 650-656.

[30] Gruenke, N. L.; Cardinal, M. F.; McAnally, M. O.; Frontiera, R. R.; Schatz, G. C.; Van Duyne, R. P. Ultrafast and Nonlinear Surface-Enhanced Raman Spectroscopy. *Chem. Soc. Rev.* **2016**, *45*, 2263-2290**.**

[31] Zheng, D.; Lu, L.; Li, Y.; Kelly, K. F.; Baldelli, S. Compressive Broad-Band Hyperspectral Sum Frequency Generation Microscopy to Study Functionalized Surfaces. *J. Phys. Chem. Lett.*, **2016**, *7*, pp 1781–1787.

[32] Di Napoli, C.; Pope, I.; Masia, F.; Langbein, W.; Watson, P.; Borri, P. Quantitative Spatiotemporal Chemical Profiling of Individual Lipid Droplets by Hyperspectral CARS Microscopy in Living Human Adipose-Derived Stem Cells. *Anal. Chem.* **2016**, *88*, 3677-3685.

[33] Kong, L.; Navas-Moreno, M.; Chan, J. W. Fast Confocal Raman Imaging Using a 2-D Multifocal Array for Parallel Hyperspectral Detection. *Anal. Chem.* **2016**, *88*, 1281-1285.

[34] El-Khoury, P. Z.; Abellan, P.; Gong, Y.; Hage, F. S.; Cottom, J.; Joly, A. G.; Brydson, R.; Ramasse, Q. M.; Hess, W. P. Visualizing Surface Plasmons with Photons, Photoelectrons, and Electrons. *Analyst* **2016**, *141*, 3562-3572.

[35] Ringe, E.; Sharma, B.; Henry, A.; Marks, L. D.; Van Duyne, R. P. Single Nanoparticle Plasmonics. *Phys. Chem. Chem. Phys.* **2013**, *15*, 4110-4129.

[36] Novo, C.; Gomez, D.; Perez-Juste, J.; Zhang, Z.; Petrova, H.; Reismann, M.; Mulvaney, P.; Hartland, G. V. Contributions from Radiation Damping and Surface Scattering to the Linewidth of the Longitudinal Plasmon Band of Gold Nanorods: A Single Particle Study. *Phys. Chem. Chem. Phys.* **2006**, *8*, 3450-3456.

[37] Tcherniak, A.; Ha, J. W.; Dominguez-Medina, S.; Slaughter, L. S.; Link, S. Probing a Century Old Prediction One Plasmonic Particle at a Time. *Nano Lett.* **2010**, *10*, 1398-1404.

[38] Fairbairn, N. ; Christofidou, A.; Kanaras, A. G.; Newman, T. A.; Muskens, O. L. Hyperspectral Darkfield Microscopy of Single Hollow Gold Nanoparticles for Biomedical Applications. *Phys. Chem. Chem. Phys.* **2013**, *15*, 4163-4168.

[39] El-Khoury, P. Z.; Joly, A. G.; Hess, W. P. Hyperspectral Dark Field Optical Microscopy of Single Silver Nanospheres. *J. Phys. Chem. C* **2016**, *120*, 7295-7298.

[40] Keller, M. D.; Selvin, R. C.; Claus, W.; Guillard, R. R. L. Media for the Culture of Oceanic Ultraphytoplankton. *J. Phycol.* **1987**, *23*, 633-638.

[41] Link, S.; El Sayed, M. A. Size and Temperature Dependence of the Plasmon Absorption of Colloidal Gold Nanoparticles. *J. Phys. Chem. B* **1999**, *103*, 4212-4217.

[42] Peppernick, S. J.; Joly, A. G.; Beck, K. M.; Hess, W. P. Plasmon-induced Optical Field Enhancement Studied by Correlated Scanning and Photoemission Electron Microscopy. *J. Chem. Phys.*, 2013, **138**, 154701-1-10.

[43] El-Khoury, P. Z.; Abellan, P.; Gong, Y.; Hage, F. S.; Cottom, J.; Joly, A. G.; Brydson, R.; Ramasse, Q. M.; Hess, W. P. Visualizing Surface Plasmons with Photons, Photoelectrons, and Electrons. *Analyst* **2016**, *141*, 3562-3572.

[44] Garnier, M.; Carrier, G.; Rogniaux, H.; Nicolau, E.; Bougaran, G.; Saint-Jean, B.; Cadoret, J. P. Comparative Proteomics Reveals Proteins Impacted by Nitrogen Deprivation in Wild-Type and High Lipid-Accumulating Mutant Strains of Tisochrysis Lutea. *J. Proteomics* **2014**, *105*, 107-120.

[45] Slocombe, S, P.; Zhang, Q. Y.; Ross, M.; Anderson, A.; Thomas, N. J.; Lapresa, A.; Rad Menéndez, C.; Campbell, C. N.; Black, K. D.; Stanley, M. S.; Day. J. G. Unlocking Nature's Treasure-Chest: Screening for Oleaginous Algae. *Sci. Rep.* **2015**, *5*, 09844-1-17.

[46] Shi, Q.; Araie, H.; Bakku, R. F.; Fukao, Y.; Rakwal, R.; Suzuki, I.; Shiraiwa, Y. Proteomic Analysis of Lipid Body from the Alkenone-Producing Marine Haptophyte Alga Tisochrysis Lutea. *Proteomics* **2015**, *15*, 4145-4158.

[47] Pilon, L.; Berberoğlu, H.; Kandilian, R. Radiation Transfer in Photobiological Carbon Dioxide Fixation and Fuel Production by Microalgae. *J. Quant. Spectrosc. Radiat. Transfer* **2011**, *112*, 2639–2660.

[48] Alkhamis, Y.; Qin, J. G. Comparison of Pigment and Proximate Compositions of Tisochrysis Lutea in Phototrophic and Mixotrophic Cultures. *J. Appl. Phycol.* **2016**, *28*, 35-42.

[49] Bendif, E. M.; Probert, I.; De Vargas, C. On the Description of Tisochrysis Lutea gen. nov sp nov and Isochrysis nuda sp nov in the Isochrysidales, and the Transfer of Dicrateria to the Prymnesiales (Haptophyta). *J. Appl. Phycol.* **2013**, *15*, 1763-1776.

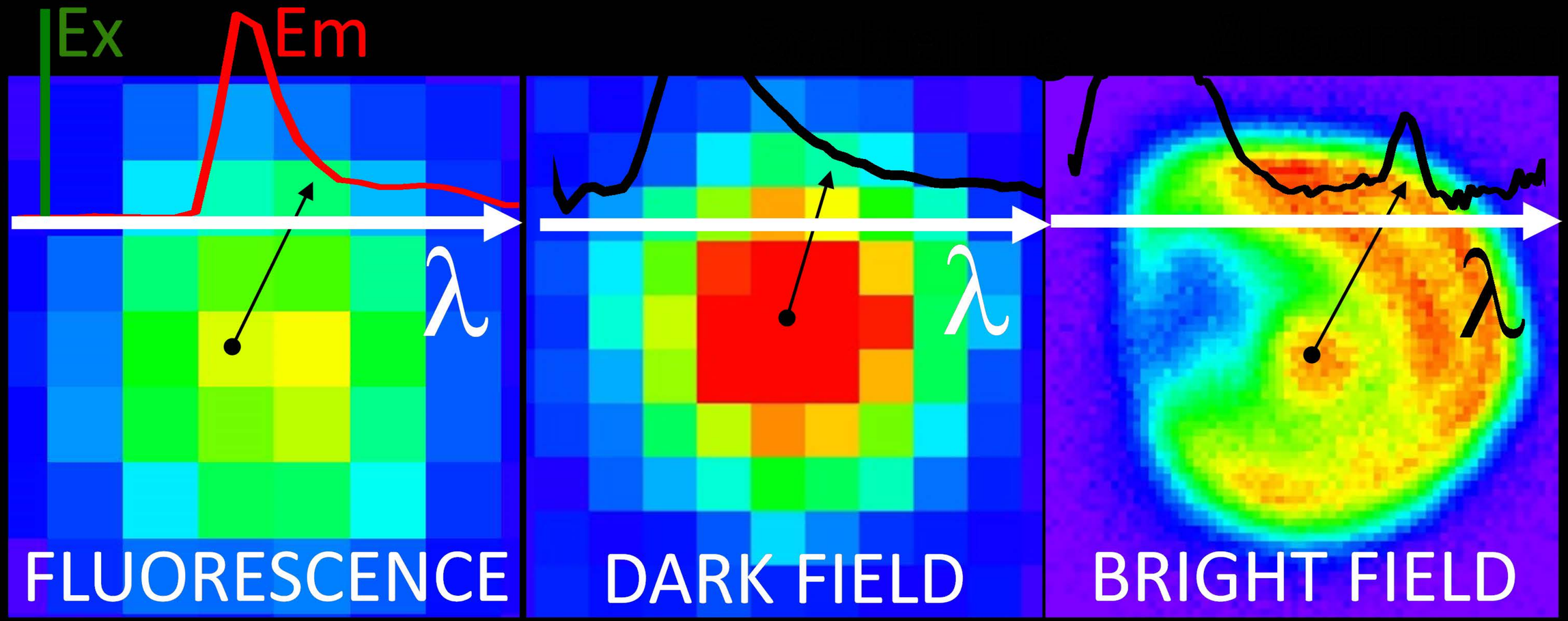
Ex
Em
λ
λ
λ
FLUORESCENCE
DARK FIELD
BRIGHT FIELD